The entropy ADC values of the selected regions of interest, which were calculated by using the volume histogram method (24,25), were obtained automatically from the same plug-in software. Entropy describes the variation in an ADC histogram such that a large variation in hepatic ADC is associated with larger entropy values.

The histogram entropy was calculated as follows:

$$\text{Entropy} = \sum (-p_i) \log(p_i),$$

where p_i represents the probability of ADC value in the image and is calculated by dividing the number of voxels in each ADC value by the number of voxels in all ADC values.

Therefore, ADC values were recorded as the mean and entropy ADC of the volume histogram obtained from the selected regions of interest.

Assessment of Pathologic Specimens

Resected liver specimens (n = 48) and liver biopsy specimens (n = 7) were fixed in formalin, embedded in paraffin, and stained with hematoxylin and eosin. All specimens (n = 55) were retrospectively reviewed independently by two pathologists (M.K. and O.N., with 34 and 26 years of experience, respectively, and subspecialty expertise in liver pathology). The pathologists were blinded to clinical and imaging data.

The fibrosis stage and the necroinflammatory activity grade were evaluated semiquantitatively by using the METAVIR scoring system (9,13,20). Fibrosis was graded on a scale of 0 to 4, as follows: F0 = no fibrosis, F1 = portal fibrosis without septa, F2 = portal fibrosis and few septa, F3 = numerous septa without cirrhosis, and F4 = cirrhosis. The necroinflammatory activity score was graded on a scale of 0 to 3, as follows: A0 = no activity, A1 = mild activity, A2 = moderate activity, and A3 = severe activity. After calculating the κ values for interobserver agreement on the basis of the independent readings, any cases in which the final fibrosis stage or activity grade differed between the two pathologists were reevaluated and scored in consensus.

Statistical Analysis

The mean and entropy ADC values of the two independent observers' measurements were compared with the Bland-Altman method (28,29). The coefficients of repeatability were calculated as 1.96 times the standard deviation of the differences between the two measurements made by the two observers. The linear correlation coefficient (r value) of each difference of measurement was calculated by using Pearson linear regression analysis, and the estimated bias (ie, the mean difference between two observers' measurements) was assessed.

Agreement between the two pathologists with regard to the fibrosis stage and inflammatory activity grade was assessed by using κ statistics (30) with use of the diagnoses made before agreement by consensus. The strength of the interobserver agreement indicated with κ values was classified as follows: poor, κ < 0.0; slight, κ = 0.0–0.20; fair, κ = 0.21–0.40; moderate, κ = 0.41–0.60; substantial, κ = 0.61–0.80; and almost perfect, κ = 0.81–1.00 (31). The relationship between the fibrosis stage and inflammatory activity grade in patients with chronic hepatitis C was assessed by using the Spearman correlation test.

The Kruskal-Wallis test was used to determine the statistical significance of intergroup differences in the pathologic scores with mean and entropy ADC. In case of statistical significance, multiple pairwise comparisons were conducted with the Mann-Whitney U test with Bonferroni correction.

The diagnostic performance of mean or entropy ADC in predicting the fibrotic stage or inflammatory activity grade was assessed with use of the area under the receiver operating characteristic curve (A_z) (32). Sensitivity, specificity, positive and negative predictive values, and positive and negative likelihood ratios (33,34) for the classification of F0 versus F1–F4 fibrosis (score ≥F1); F0 and F1 versus F2–F4 fibrosis (score ≥F2); F0–F2 versus F3 and F4 fibrosis (score ≥F3); or F0–F3 versus F4 fibrosis (score = F4) and for the classification of A0 versus A1–A3 activity (grade ≥A1); A0 and A1 versus A2 and A3 activity (grade ≥A2); or A0–A2 versus A3 activity (grade = A3) were calculated with standard formulas according to the values of these indexes and with varied index values that indicated positive differentiation (ie, threshold values).

All analyses were performed with statistical software (SPSS, version 12.0J; SPSS, Chicago, Ill), and $P < .05$ was considered indicative of a statistically significant difference.

Results

Interobserver Agreement

There was no significant difference between measurements made by the two observers for the two parameters; the interclass Pearson correlation coefficients were 0.98 (95% confidence interval [CI]: 0.95, 1.0) for mean ADC and 0.97 (95% CI: 0.94, 1.0) for entropy ADC; the mean difference (±standard deviation) was −0.004 ± 0.05 for mean ADC and −0.013 ± 0.037 for entropy ADC; and the coefficients of repeatability were 0.100 for mean ADC and 0.072 for entropy ADC. Bland-Altman plots with 95% limits of agreement for mean and entropy ADC are shown in Figure 2a and Figure 2b, respectively. There was no proportional bias or fixed bias in each Bland-Altman plot for the two parameters.

There was substantial agreement between the two independent pathologists with regard to fibrosis stage (κ = 0.73; 95% CI: 0.59, 0.86) and inflammatory activity grade (κ = 0.74; 95% CI: 0.60, 0.88). None of the 12 control subjects had any signs of fibrosis or inflammatory activity because they did not have hepatic impairment. At the consensus reading, stage F0 fibrosis was diagnosed in 12 of the 55 patients (22%), stage F1 fibrosis in nine (16%), stage F2 fibrosis in 11 (20%), stage F3 fibrosis in 11 (20%), and stage F4 fibrosis in 12 (22%), showing a homogeneous distribution of fibrosis stages. The inflammatory activity grade was A0 in 12 of the 55 patients (22%), A1 in 13 (24%), A2 in 17 (31%), and A3 in 13 (24%). In the 43 patients with chronic hepatitis C, a significant correlation

Figure 2

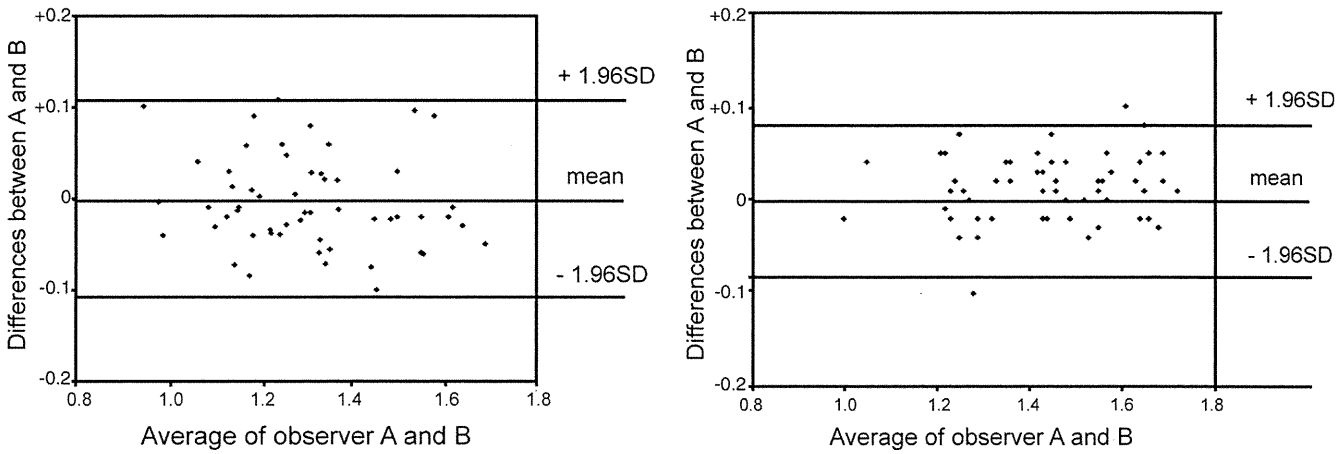

Figure 2: Bland-Altman plots depict measurements of **(a)** mean ADC (in $\times 10^{-3}$ mm²/sec) and **(b)** entropy ADC in liver parenchyma, demonstrating good interobserver agreement and lack of proportional bias or fixed bias. The average of the measurements made by the two observers is plotted against the difference between the measurements made by the two observers. The thin lines represent the mean value of all differences between the two observers, and the thick lines represent the 95% limits of agreement. *SD* = standard deviation.

was observed between the final fibrosis score and the final inflammatory activity grade ($r = 0.46$, $P = .002$, Spearman correlation test).

Relationship between ADC Parameters and Pathologic Fibrosis Stage

The median mean ADC values according to fibrosis stage were as follows: F0, 1.53×10^{-3} mm²/sec (IQR, $1.35–1.60 \times 10^{-3}$ mm²/sec); F1, 1.45×10^{-3} mm²/sec (IQR, $1.34–1.51 \times 10^{-3}$ mm²/sec); F2, 1.29×10^{-3} mm²/sec (IQR, $1.23–1.34 \times 10^{-3}$ mm²/sec); F3, 1.17×10^{-3} mm²/sec (IQR, $1.14–1.25 \times 10^{-3}$ mm²/sec); and F4, 1.15×10^{-3} mm²/sec (IQR, $1.01–1.26 \times 10^{-3}$ mm²/sec) (Fig 3a). The median entropy ADC values according to fibrosis stage were as follows: F0, 1.24 (IQR, 1.21–1.27); F1, 1.36 (IQR, 1.30–1.49); F2, 1.46 (IQR, 1.35–1.55); F3, 1.55 (IQR, 1.45–1.61); and F4, 1.64 (IQR, 1.45–1.68) (Fig 3b).

The mean ADC decreased with an increase in the stage of liver fibrosis ($P < .001$, Kruskal-Wallis test; Fig 3a). Conversely, the entropy ADC increased with an increase in fibrosis stage ($P < .001$, Kruskal-Wallis test; Fig 3b).

For the mean ADC, there were statistically significant differences in the pairwise comparisons (with Bonferroni correction) of stages of liver fibrosis, as follows: F0 versus F2, $P = .01$; F0 versus F3, $P < .01$; F0 versus F4, $P < .01$; F1 versus F3, $P < .01$; F1 versus F4, $P < .01$; F2 versus F3, $P = .04$; and F2 versus F4, $P = .04$ (Fig 3a). For the entropy ADC, there were statistically significant differences in the pairwise comparisons (Bonferroni correction) of stages of liver fibrosis, as follows: F0 versus F1, $P < .01$; F0 versus F2, $P < .01$; F0 versus F3, $P < .01$; and F1 versus F4, $P = .04$ (Fig 3b).

Relationship between ADC Parameters and Pathologic Inflammatory Activity Grade

The median mean ADC values according to inflammatory activity grade were as follows: A0, 1.53×10^{-3} mm²/sec (IQR, $1.36–1.60 \times 10^{-3}$ mm²/sec); A1, 1.30×10^{-3} mm²/sec (IQR, $1.21–1.51 \times 10^{-3}$ mm²/sec); A2, 1.26×10^{-3} mm²/sec (IQR, $1.19–1.34 \times 10^{-3}$ mm²/sec); and A3, 1.15×10^{-3} mm²/sec (IQR, $1.04–1.22 \times 10^{-3}$ mm²/sec) (Fig 4a). The median entropy ADC values according to activity grade were as follows: A0, 1.23 (IQR, 1.21–1.27); A1, 1.48 (IQR, 1.43–1.64); A2, 1.44 (IQR, 1.33–1.55); and A3, 1.57 (IQR, 1.50–1.67) (Fig 4b).

The mean ADC decreased with an increase in the inflammatory activity grade ($P < .001$, Kruskal-Wallis test; Fig 4a), and the entropy ADC increased with an increase in the inflammatory activity grade ($P < .001$, Kruskal-Wallis test; Fig 4b).

The mean ADC significantly differed between activity grades A0 and A2 and between activity grades A0 and A3 ($P < .01$ for both comparisons, Bonferroni correction) (Fig 4a). The entropy ADC significantly differed between inflammatory activity grade A0 and activity grades A1, A2, and A3 ($P < .01$ for all comparisons, Bonferroni correction) (Fig 4b).

Receiver Operating Characteristic Analyses and Diagnostic Performances for Predicting Pathologic Fibrosis and Activity Scores

The A_z values for mean and entropy ADCs according to different fibrosis and inflammatory activity thresholds are shown in Tables 1 and 2. Optimal cutoff values for mean and entropy ADC, along with the respective diagnostic performances, are shown in Tables 3 and 4.

The A_z for mean ADC was larger than that for entropy ADC in the classification of fibrosis of grade F2 or higher, fibrosis of grade F3 or higher, and fibrosis of grade F4 (Table 1). In

Figure 3

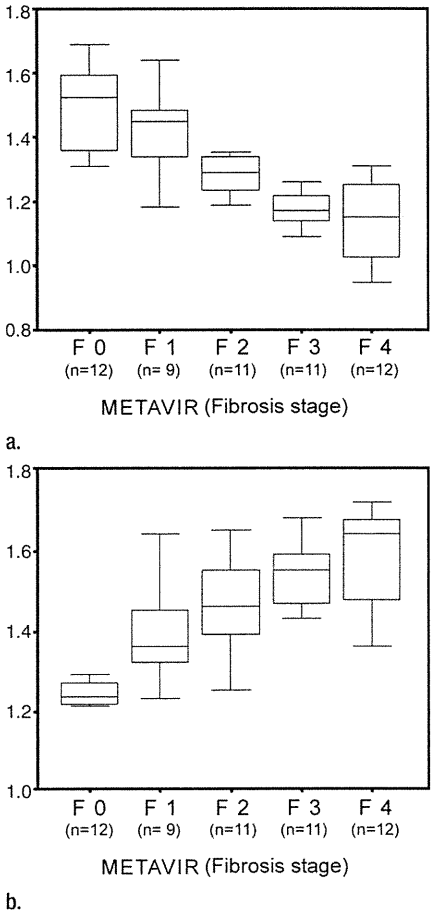

Figure 3: Box plots of **(a)** mean ADC (in $\times 10^{-3}$ mm^2/sec) and **(b)** entropy ADC values in liver parenchyma according to METAVIR fibrosis score. The line in each box represents the median, and the horizontal boundaries of the boxes represent the first and third quartiles. The vertical error bars show the minimum and maximum values (range).

Figure 4

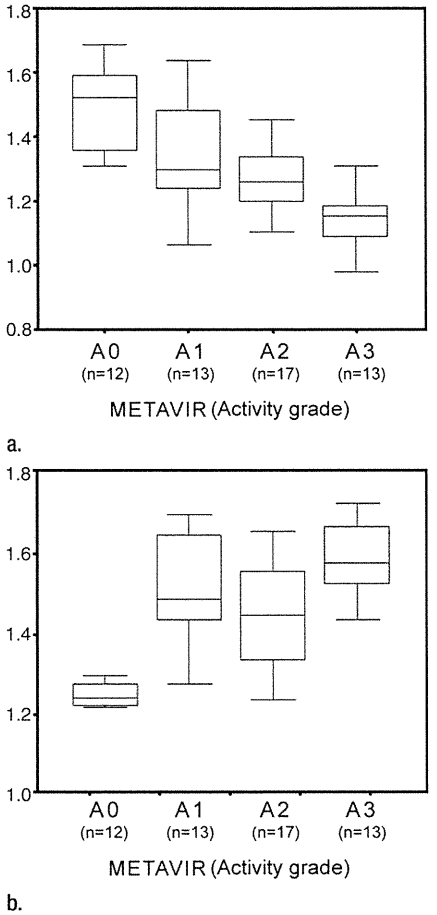

Figure 4: Box plots of **(a)** mean ADC (in $\times 10^{-3}$ mm^2/sec) and **(b)** entropy ADC values in liver parenchyma according to METAVIR inflammatory activity score. The line in each box represents the median, and the horizontal boundaries of the boxes represent the first and third quartiles. The vertical error bars show the minimum and maximum values (range).

particular, diagnostic performances in the classification of grade F2 or higher fibrosis and grade F3 or higher fibrosis were quite good (cutoff values of 1.32 and 1.27 $\times$ 10^{-3} mm^2/sec resulted in positive likelihood ratios of 9.0 and 5.6, respectively, and negative likelihood ratios of 0.16 and 0.15) (Table 3). Conversely, in the classification of fibrosis of grade F1 or higher, the A_z of entropy ADC was larger than that of mean ADC (Table 1). Thus, with regard to the diagnostic performance, entropy ADC was the most accurate parameter in the classification of grade F1 or higher fibrosis (cutoff value of 1.30 resulted in a positive likelihood ratio of 10.6 and negative likelihood ratio of 0.13). Similarly, the A_z of mean ADC was larger than that of entropy ADC in the classification of inflammatory activity of grade A2 or higher and grade A3 or higher. For inflammatory activity of at least grade A1, the A_z of entropy ADC was larger than that of mean ADC (Table 2). With regard to the diagnostic performance, entropy ADC was the most accurate parameter in the classification of inflammatory activity of grade A1 or higher (cutoff value of 1.30 resulted in a positive likelihood ratio of 10.9 and negative likelihood ratio of 0.10), and mean ADC was a relatively significant predictor for classification of grade A3 inflammatory activity (cutoff value of 1.19 $\times$ 10^{-3} mm^2/sec resulted in a positive likelihood ratio of 4.6 and negative likelihood ratio of 0.28) (Table 4).

Discussion

Early studies assessing the relationship between hepatic fibrosis stage and ADC values in the liver reported that a significant correlation was not achieved when using low *b* values (eg, 0–128 sec/mm^2 and 50–400 sec/mm^2) (15,18,19) because DW MR imaging with a low *b* value was influenced by perfusion contamination. Taouli et al (20) reported that the ADC value acquired from *b* values of at least 500 sec/mm^2 showed a significant correlation with the liver fibrosis stage and that the ADC value with a combination of *b* values of 0–1000 sec/mm^2 showed the highest significant correlation with fibrosis stage. On the basis of the study of combined ADC measurement with multiple *b* values (0, 200, 400, 800 sec/mm^2), Luciani et al (35) reported that ADC changes observed in liver cirrhosis (METAVIR fibrosis score, F4) were more reflective of an alteration in microperfusion than of true diffusion. Although the use of multiple *b* values (intravoxel incoherent motion) may be helpful for differentiating the relative effect of altered microperfusion from that of true diffusion due to increased barriers to water movement, as suggested by Luciani et al, our results are consistent with those of other studies (15,20,21) that demonstrated that liver ADC derived from a combination of *b* values of 0 and 1000 sec/mm^2 is helpful for predicting hepatic fibrosis. The different correlations of ADC parameters and pathologic findings in our study compared with that of Luciani et al (35) may be explained in part by different patient populations; the patient population in the study by Luciani et al consisted of patients with cirrhosis (12 patients

with grade F4 fibrosis). Further studies (including those performed in patients with chronic hepatitis with a fibrosis score lower than F4) are needed to confirm these findings and shed light on the exact mechanism of diffusion changes observed in liver fibrosis (22).

Previous studies have reported a range of liver ADC sensitivities of 0.74–0.89 and specificities of 0.73–0.87 in the detection of moderate fibrosis (stage F2 or higher) (15,19,21). These findings concur with our observation of mean ADC sensitivity (0.85) and specificity (0.91); however, we observed a greater specificity (0.92) with entropy ADC when including even early liver fibrosis.

Although Lewin et al (15) and Taouli et al (21) reported weak negative correlations between ADC values and the degree of necroinflammation, with a sensitivity of 0.75 and a specificity of 0.78, we observed a stronger negative correlation between mean ADC and inflammatory activity grade (sensitivity, 0.81; specificity, 0.83). In addition, entropy, which is a measure of the variability in the volume histogram analyses of the ADC values, showed a greater correlation with the fibrosis stage and inflammatory activity grade than did mean ADC, with a sensitivity of 0.91 and a specificity of 0.92 in the detection of inflammation.

In patients with chronic hepatitis C, a significant correlation between the pathologic fibrosis stage and the inflammatory activity grade is well known (36,37). Our results are consistent with those results and indicate that fibrosis tends to evolve as necroinflammation becomes more pronounced in chronic hepatitis C. Although the Spearman coefficient value was relatively low (r = 0.46), this trend may be one of the reasons why liver ADC showed an inverse correlation with both fibrosis stage and inflammatory activity grade. The possible biologic implications of a reduced mean ADC value and an increased entropy ADC value with increasing fibrosis stage and inflammation are intracellular alterations, changes of cellular composition, and decreased interstitial fluids according to the fibrosis stage and inflammatory activity grade.

Table 1

A_z Values for Mean and Entropy ADC according to METAVIR Fibrosis Score

Parameter	≥F1	≥F2	≥F3	F4
Mean ADC	0.889 (0.799, 0.978)	0.925 (0.851, 0.999)	0.926 (0.859, 0.993)	0.842 (0.730, 0.954)
Entropy ADC	0.937 (0.855, 1.0)	0.882 (0.787, 0.978)	0.855 (0.759, 0.950)	0.815 (0.675, 0.954)

Note.—Data are given as mean A_z values. Numbers in parentheses are 95% CIs. $P < .001$ for all comparisons.

Table 2

A_z Values for Mean and Entropy ADC according to METAVIR Activity Grade

Parameter	≥A1	≥A2	A3
Mean ADC	0.889 (0.799, 0.978)	0.807 (0.690, 0.925)	0.842 (0.722, 0.961)
Entropy ADC	0.937 (0.855, 1.0)	0.697 (0.554, 0.841)*	0.808 (0.691, 0.925)

Note.—Data are given as mean A_z values. Numbers in parentheses are 95% CIs. Except where indicated, $P < .001$.

* $P = .012$.

Our data highlight entropy ADC as a sensitive marker of overall hepatic damage that strongly correlated to pathologic fibrosis stage and inflammatory activity grade in patients with chronic hepatitis C. The most prominent finding of our study is the difference in entropy ADC values between patients without any signs of fibrosis (stage F0) and those with fibrosis of any pathologic stage (stages F1–F4) and between patients without inflammatory activity (grade A0) and those with any grade of inflammatory activity (grades A1–A3). Although other studies using entropy have not been performed in the abdomen, studies in patients with multiple sclerosis have shown that entropy can help measure macroscopic and microscopic tissue changes in the brain (25,26); neurologic damage has been reportedly associated with increased heterogeneity of signal intensities at DW imaging of the brain (25,26). As the distribution of these signal intensities becomes more heterogeneous (and the image therefore more random), entropy increases. Histopathologically, early fibrosis and inflammatory activity in chronic viral hepatitis demonstrate mild portal fibrosis and mild piecemeal necrosis and/or lobular necrosis (9,37) in addition to vascular changes (damage and disappearance of some branches of the portal veins) (38). In viral hepatitis, liver fibrosis begins in the portal triads and extends into the surrounding hepatic parenchyma. Thickening and lengthening of the fibrous septa results in the formation of fibrous bridges that link adjacent portal triads and central veins. With progressive liver injury, the bridges continue to enlarge and coalesce and eventually divide the liver into rounded islands of hepatic parenchyma (regenerative nodules) surrounded by fibrosis tissue. The change in tissue composition and architecture may be expected to increase barriers to water movement. The deposition of fibrous tissue leads to a reduction in the size or obliteration of small venules, with a resultant increase in portal venous pressure and consequent compensatory increased arterial blood flow. Changes in regional liver perfusion may have contributed to the increase in entropy ADC we observed in the early stages of liver disease. Infiltration of inflammatory cells into the liver interstitial tissue would also be expected to reduce water movement and increase liver ADC with regional variation. Regardless of early stage and grade, when these changes are combined, it causes the liver to go to a structure with an unstable architectural state according to chronic liver injury, from a normal structure with orderly normal tissue. The observation of increased liver entropy ADC depicted by means of the increased variability of ADC at

Table 3

Performance of Mean and Entropy ADC in the Prediction of METAVIR Fibrosis Score according to Cutoff Values

Parameter*	≥F1	≥F2	≥F3	F4
Cutoff mean ADC ($\times 10^{-3}$ mm²/sec)	1.35	1.32	1.27	1.23
Sensitivity	0.79 (0.64, 0.90)	0.85 (0.69, 0.95)	0.87 (0.66, 0.97)	0.75 (0.43, 0.95)
Specificity	0.83 (0.52, 0.98)	0.91 (0.70, 0.99)	0.84 (0.67, 0.95)	0.72 (0.56, 0.85)
PPV	0.94 (0.81, 0.99)	0.94 (0.79, 0.99)	0.80 (0.59, 0.93)	0.43 (0.22, 0.66)
NPV	0.53 (0.29, 0.76)	0.79 (0.58, 0.93)	0.90 (0.73, 0.98)	0.91 (0.76, 0.98)
Positive LR	4.7 (1.8, 16.7)	9.0 (3.2, 30.7)	5.6 (2.9, 9.4)	2.7 (1.4, 3.8)
Negative LR	0.25 (0.19, 0.47)	0.16 (0.11, 0.31)	0.15 (0.06, 0.36)	0.35 (0.12, 0.76)
Cutoff entropy ADC	1.30	1.43	1.48	1.58
Sensitivity	0.88 (0.72, 0.97)	0.82 (0.65, 0.93)	0.74 (0.52, 0.90)	0.67 (0.35, 0.090)
Specificity	0.92 (0.62, 0.99)	0.86 (0.64, 0.97)	0.78 (0.61, 0.89)	0.88 (0.75, 0.96)
PPV	0.97 (0.83, 0.995)	0.90 (0.74, 0.98)	0.71 (0.49, 0.87)	0.62 (0.31, 0.86)
NPV	0.69 (0.41, 0.89)	0.75 (0.53, 0.90)	0.81 (0.63, 0.93)	0.90 (0.77, 0.97)
Positive LR	10.6 (2.7, 58.8)	5.8 (2.5, 15.5)	3.4 (1.8, 6.1)	5.7 (2.4, 12.0)
Negative LR	0.13 (0.10, 0.25)	0.21 (0.13, 0.38)	0.33 (0.18, 0.61)	0.38 (0.18, 0.69)

Note.—Numbers in parentheses are 95% CIs.

* LR = likelihood ratio, NPV = negative predictive value, PPV = positive predictive value.

Table 4

Performance of Mean and Entropy ADC in the Prediction of METAVIR Inflammatory Activity Score according to Cutoff Values

Parameter*	≥A1	≥A2	A3
Cutoff mean ADC value ($\times 10^{-3}$ mm²/sec)	1.35	1.28	1.19
Sensitivity	0.81 (0.67, 0.92)	0.73 (0.54, 0.88)	0.77 (0.46, 0.95)
Specificity	0.83 (0.52, 0.98)	0.80 (0.59, 0.93)	0.83 (0.69, 0.93)
PPV	0.95 (0.82, 0.99)	0.81 (0.62, 0.94)	0.59 (0.33, 0.82)
NPV	0.56 (0.31, 0.78)	0.71 (0.51, 0.87)	0.92 (0.79, 0.98)
Positive LR	4.8 (1.8, 17.1)	3.7 (1.8, 7.9)	4.6 (2.3, 7.4)
Negative LR	0.22 (0.16, 0.43)	0.33 (0.21, 0.58)	0.28 (0.10, 0.60)
Cutoff entropy ADC value	1.30	1.43	1.51
Sensitivity	0.91 (0.78, 0.97)	0.73 (0.54, 0.88)	0.77 (0.46, 0.95)
Specificity	0.92 (0.62, 0.99)	0.60 (0.39, 0.79)	0.76 (0.61, 0.88)
PPV	0.98 (0.87, 0.99)	0.69 (0.50, 0.84)	0.50 (0.27, 0.73)
NPV	0.73 (0.45, 0.92)	0.65 (0.43, 0.84)	0.91 (0.77, 0.98)
Positive LR	10.9 (2.8, 59.7)	1.8 (1.1, 3.0)	3.2 (1.7, 4.7)
Negative LR	0.10 (0.08, 0.22)	0.44 (0.23, 0.84)	0.30 (0.11, 0.67)

Note.—Numbers in parentheses are 95% CIs.

* LR = likelihood ratio, NPV = negative predictive value, PPV = positive predictive value.

volumetric histogram analysis may therefore be a potential biomarker that reflects increased heterogeneity of hepatic parenchyma in diffuse liver disease. Furthermore, entropy ADC may be more helpful than mean ADC alone for detecting early stage fibrosis and early inflammatory activity.

There are a few limitations to our study. First, the study was retrospective and involved a small number of patients. A prospective study with a substantially larger sample is needed to further validate our findings. Second, because the pathologic specimens were obtained at surgery for a hepatic mass or with core biopsy, exact mapping of pathologic findings and imaging was not possible. However, our study was targeted at evaluating diffuse hepatic disease rather than characterizing focal lesions. Third, DW MR imaging is susceptible to motion artifacts that may interfere with quantitative measurements. We used respiratory-triggered DW MR imaging to reduce respiratory artifacts. The use of mean ADC and volumetric acquisition for entropy ADC should result in averaging of signal intensities to provide some compensation for respiratory motion. In addition, all measurements were obtained in the right lobe of the liver because the left lobe exhibits greater motion-related artifact. However, core liver biopsy, which is often used as the standard for staging the severity of liver disease, is also performed from the right lobe of the liver. Fourth, we used a combination of *b* values of 0 and 1000 sec/mm² for DW imaging. Further studies using a combination of at least three *b* values might be needed.

In summary, our data suggest that the diagnostic performance of mean or entropy ADC for predicting pathologic stage or inflammatory grade is at least similar to that of other DW MR imaging studies (22); however, the combination of mean and entropy ADC may improve diagnostic performances, particularly in the detection of inflammatory activity in the liver.

In practical clinical use, the evaluation with mean and entropy ADC may have several advantages: *(a)* The noninvasive nature of the examination allows for repeat performance; *(b)* entropy ADC may be able to help differentiate normal from any abnormal fibrosis stage or abnormal inflammatory activity grade and, thus, may represent indexes at the initiation of treatment and of improvement after treatment; and *(c)* mean ADC may reflect abnormal fibrosis stage (especially ≥F2 and ≥F3) and, thus, may help determine disease severity and the effects of therapy performed to treat hepatic fibrosis.

In conclusion, our preliminary data suggest that mean and entropy ADC might be helpful for predicting pathologic hepatic fibrosis stage and inflammatory activity grade in patients with chronic hepatitis C.

Disclosures of Potential Conflicts of Interest: K.F. Financial activities related to the present article: none to disclose. Financial activities not related to the present article: none to disclose. Other relationships: none to disclose. **T.T.** Financial activities related to the present article: none to disclose. Financial activities not related to the present article: none to disclose. Other relationships: none to disclose. **S.A.** Financial activities related to the present article: none to disclose. Financial activities not related to the present article: none to disclose. Other relationships: none to disclose. **M.K.** Financial activities related to the present article: none to disclose. Financial activities not related to the present article: none to disclose. Other relationships: none to disclose. **O.N.** Financial activities related to the present article: none to disclose. Financial activities not related to the present article: none to disclose. Other relationships: none to disclose. **T.J.** Financial activities related to the present article: none to disclose. Financial activities not related to the present article: none to disclose. Other relationships: none to disclose. **N.H.** Financial activities related to the present article: none to disclose. Financial activities not related to the present article: none to disclose. Other relationships: none to disclose. **K.O.** Financial activities related to the present article: none to disclose. Financial activities not related to the present article: none to disclose. Other relationships: none to disclose. **T.K.** Financial activities related to the present article: none to disclose. Financial activities not related to the present article: none to disclose. Other relationships: none to disclose. **M.S.** Financial activities related to the present article: none to disclose. Financial activities not related to the present article: none to disclose. Other relationships: none to disclose. **A.Q.** Financial activities related to the present article: none to disclose. Financial activities not related to the present article: none to disclose. Other relationships: none to disclose.

References

1. Ezelle HJ, Markovic D, Barber GN. Generation of hepatitis C virus–like particles by use of a recombinant vesicular stomatitis virus vector. J Virol 2002;76(23):12325–12334.
2. Afdhal NH. The natural history of hepatitis C. Semin Liver Dis 2004;24(suppl 2):3–8.
3. Strader DB, Wright T, Thomas DL, Seeff LB; American Association for the Study of Liver Diseases. Diagnosis, management, and treatment of hepatitis C. Hepatology 2004;39(4):1147–1171.
4. Tsukuma H, Hiyama T, Tanaka S, et al. Risk factors for hepatocellular carcinoma among patients with chronic liver disease. N Engl J Med 1993;328(25):1797–1801.
5. Hofmann WP, Zeuzem S, Hepatitis C. Hepatitis C: new therapeutic strategies needed for advanced disease. Nat Rev Gastroenterol Hepatol 2009;6(6):325–327.
6. Manning DS, Afdhal NH. Diagnosis and quantitation of fibrosis. Gastroenterology 2008;134(6):1670–1681.
7. Batts KP, Ludwig J. Chronic hepatitis: an update on terminology and reporting. Am J Surg Pathol 1995;19(12):1409–1417.
8. Knodell RG, Ishak KG, Black WC, et al. Formulation and application of a numerical scoring system for assessing histological activity in asymptomatic chronic active hepatitis. Hepatology 1981;1(5):431–435.
9. Ishak K, Baptista A, Bianchi L, et al. Histological grading and staging of chronic hepatitis. J Hepatol 1995;22(6):696–699.
10. Intraobserver and interobserver variations in liver biopsy interpretation in patients with chronic hepatitis C. The French METAVIR Cooperative Study Group. Hepatology 1994;20(1 pt 1):15–20.
11. Rozario R, Ramakrishna B. Histopathological study of chronic hepatitis B and C: a comparison of two scoring systems. J Hepatol 2003;38(2):223–229.
12. Talwalkar JA, Yin M, Fidler JL, Sanderson SO, Kamath PS, Ehman RL. Magnetic resonance imaging of hepatic fibrosis: emerging clinical applications. Hepatology 2008;47(1):332–342.
13. Mallet V, Gilgenkrantz H, Serpaggi J, et al. Brief communication: the relationship of regression of cirrhosis to outcome in chronic hepatitis C. Ann Intern Med 2008;149(6):399–403.
14. Friedrich-Rust M, Wunder K, Kriener S, et al. Liver fibrosis in viral hepatitis: noninvasive assessment with acoustic radiation force impulse imaging versus transient elastography. Radiology 2009;252(2):595–604.
15. Lewin M, Poujol-Robert A, Boëlle PY, et al. Diffusion-weighted magnetic resonance imaging for the assessment of fibrosis in chronic hepatitis C. Hepatology 2007;46(3):658–665.
16. Lucidarme O, Baleston F, Cadi M, et al. Noninvasive detection of liver fibrosis: is superparamagnetic iron oxide particle–enhanced MR imaging a contributive technique? Eur Radiol 2003;13(3):467–474.
17. Aguirre DA, Behling CA, Alpert E, Hassanein TI, Sirlin CB. Liver fibrosis: noninvasive diagnosis with double contrast material–enhanced MR imaging. Radiology 2006;239(2):425–437.
18. Koinuma M, Ohashi I, Hanafusa K, Shibuya H. Apparent diffusion coefficient measurements with diffusion-weighted magnetic resonance imaging for evaluation of hepatic fibrosis. J Magn Reson Imaging 2005;22(1):80–85.
19. Sandrasegaran K, Akisik FM, Lin C, et al. Value of diffusion-weighted MRI for assessing liver fibrosis and cirrhosis. AJR Am J Roentgenol 2009;193(6):1556–1560.
20. Taouli B, Tolia AJ, Losada M, et al. Diffusion-weighted MRI for quantification of liver fibrosis: preliminary experience. AJR Am J Roentgenol 2007;189(4):799–806.
21. Taouli B, Chouli M, Martin AJ, Qayyum A, Coakley FV, Vilgrain V. Chronic hepatitis: role of diffusion-weighted imaging and diffusion tensor imaging for the diagnosis of liver fibrosis and inflammation. J Magn Reson Imaging 2008;28(1):89–95.
22. Taouli B, Koh DM. Diffusion-weighted MR imaging of the liver. Radiology 2010;254(1):47–66.
23. Girometti R, Furlan A, Esposito G, et al. Relevance of *b*-values in evaluating liver fibrosis: a study in healthy and cirrhotic subjects using two single-shot spin-echo echo-planar diffusion-weighted sequences. J Magn Reson Imaging 2008;28(2):411–419.
24. Huwart L, Sempoux C, Vicaut E, et al. Magnetic resonance elastography for the noninvasive staging of liver fibrosis. Gastroenterology 2008;135(1):32–40.
25. Benedict RH, Bruce J, Dwyer MG, et al. Diffusion-weighted imaging predicts cognitive impairment in multiple sclerosis. Mult Scler 2007;13(6):722–730.
26. Tavazzi E, Dwyer MG, Weinstock-Guttman B, et al. Quantitative diffusion weighted imaging measures in patients with multiple sclerosis. Neuroimage 2007;36(3):746–754.
27. WMA Declaration of Helsinki—Ethical Principles for Medical Research Involving Human Subjects. Amended by the 59th WMA General Assembly, Seoul, October 2008. World Medical Association. http://www.wma.net/en/30publications/10policies/b3/index.html. Updated October 22, 2008. Accessed January 10, 2010.
28. Bland JM, Altman DG. Statistical methods for assessing agreement between two methods of clinical measurement. Lancet 1986;1(8476):307–310.
29. Ludbrook J. Statistical techniques for comparing measurers and methods of measurement:

a critical review. Clin Exp Pharmacol Physiol 2002;29(7):527–536.

30. Kundel HL, Polansky M. Measurement of observer agreement. Radiology 2003;228(2):303–308.

31. Landis JR, Koch GG. The measurement of observer agreement for categorical data. Biometrics 1977;33(1):159–174.

32. DeLong ER, DeLong DM, Clarke-Pearson DL. Comparing the areas under two or more correlated receiver operating characteristic curves: a nonparametric approach. Biometrics 1988;44(3):837–845.

33. Jaeschke R, Guyatt GH, Sackett DL. Users' guides to the medical literature. III. How to use an article about a diagnostic test. B. What are the results and will they help me in caring for my patients? The Evidence-Based Medicine Working Group. JAMA 1994;271(9):703–707.

34. Fritz JM, Wainner RS, Wainner RS. Examining diagnostic tests: an evidence-based perspective. Phys Ther 2001;81(9):1546–1564.

35. Luciani A, Vignaud A, Cavet M, et al. Liver cirrhosis: intravoxel incoherent motion MR imaging—pilot study. Radiology 2008;249(3):891–899.

36. Yano M, Kumada H, Kage M, et al. The long-term pathological evolution of chronic hepatitis C. Hepatology 1996;23(6):1334–1340.

37. Kage M, Fujisawa T, Shiraki K, et al. Pathology of chronic hepatitis C in children. Child Liver Study Group of Japan. Hepatology 1997;26(3):771–775.

38. Hano H, Takasaki S. Three-dimensional observations on the alterations of lobular architecture in chronic hepatitis with special reference to its angioarchitecture for a better understanding of the formal pathogenesis of liver cirrhosis. Virchows Arch 2003;443(5):655–663.

Pediatr Surg Int
DOI 10.1007/s00383-011-2974-5

ORIGINAL ARTICLE

The herbal medicine Inchinko-to reduces hepatic fibrosis in cholestatic rats

Takahiro Asakawa · Minoru Yagi · Yoshiaki Tanaka · Kimio Asagiri · Hidefumi Kobayashi · Hideaki Egami · Ken Tanikawa · Masayoshi Kage

Accepted: 5 September 2011

Abstract
Purpose Several studies have reported the herbal medicine Inchinko-to (ICKT) to have an antifibrotic effect which thus leads to an improvement of hepatic injury. However, there are still few reports of its use in the treatment of cholestatic liver disorder. The aim of this study was to clarify whether the administration of ICKT will ameliorate hepatic fibrosis and injury in cholestatic rats.
Materials and methods We performed bile duct ligation on 7-week-old male cholestatic Wistar rats and assigned them to one of three groups according to the method of treatment : (1) the SHAM group, (2) the NT-group (non-treatment group), and (3) the T-group (treatment-group). Rats in the T-group were orally administered ICKT (TJ-135) at a dose of 1 g/kg/day and were killed on the 17th postoperative day. We subsequently investigated the levels of fibrosis and various clinical markers through measurement of the following: serum levels of AST and ALT; tissue transforming growth factor-beta 1 (TGF-beta1); tissue inhibitor metalloprotease-1 mRNA (TIMP-1 mRNA) through real-time PCR analysis; and Azan staining and immunohistochemical staining of alfa-smooth muscle actin (alfa-SMA) to evaluate the degree of fibrosis.
Results The levels of serum AST, serum ALT, and TGF-bata1 in the T-Group were significantly lower than those in the NT-Group. In addition, staining of Azan and alfa-SMA in the T-Group was significantly lower than those in the NT-Group.
Conclusion ICKT may help reduce hepatic fibrosis and injury by controlling stellate cell activation.

Keywords Inchinko-to · Antifibrotic effect · Hepatic fibrosis · Cholestasis · Biliary atresia

Background

Many patients with biliary atresia (BA) continue to suffer from postoperative liver dysfunction, even after undergoing Kasai's hepatic portoenterostomy. Such patients can experience chronic inflammation with or without jaundice. The prevention of progressive liver fibrosis has, therefore, become an important factor to achieve favorable long-term results. For this purpose, a combination of medications that have hepatocyte protective activity has been used routinely in post-operative patients with BA. The herbal medicine Inchinko-to (ICKT) has been commonly used in Japan as an anti-inflammatory, antipyretic, choleretic, and diuretic agent for liver disorders and jaundice [1–3]. Recently, ICKT has been reported to have a potent inhibitory effect on hepatocyte apoptosis, induced by transforming growth factor-beta 1 (TGF-beta1), and it inhibits the production of inflammatory cytokines in concanavalin A-induced hepatitis [4, 5]. Furthermore, ICKT has been reported to directly suppress liver fibrosis in vivo [6, 7]. Clinical reports in Japan also suggest that

T. Asakawa (✉) · M. Yagi · Y. Tanaka · K. Asagiri · H. Kobayashi
Department of Pediatric Surgery, Kurume University School of Medicine, 67 Asahimachi, Kurume, Fukuoka 830-0011, Japan
e-mail: monmon@ka3.so-net.ne.jp

H. Egami
Department of Innovative Kampo Medicine, Kurume University School of Medicine, Kurume, Japan

K. Tanikawa · M. Kage
Department of Pathology, Kurume University School of Medicine, 67 Asahimachi, Kurume, Fukuoka 830-0011, Japan

Published online: 02 November 2011

ICKT might be beneficial for the treatment of hepatobiliary diseases in adults [7]. These models in vivo had made by the injection of carbon tetrachloride (CCl_4) or pig-serum. However, those reports have not been validate in cholestatic liver disorders [6–8].

The pathologic mechanism of the progression from cholestasis to fibrosis might be summarized as an extracellular matrix chemical imbalance caused by the activation of transcription factors and hepatic stellate cells. Continuous inflammation increases the expression of adhesion factors, which results in the accumulation of immune cells in the liver. The subsequent accumulation of hydrophobic bile acid leads to the activation of Kupffer cells, as well as the excessive production of active-oxygen species and consequent lipoperoxidation [9–11].

The aim of this study was to clarify whether the administration of ICKT can reduce hepatic fibrosis and injury in cholestatic rats.

Materials and methods

We utilized 7-week-old male Wistar rats weighing 250–300 g. Three days before the operation, we initiated intragastric administration of ICKT at a dose of 1 g/kg/day. We decided the applied dose of ICKT referring from Yamashiki et al. and Imanishi et al. [5, 12] reports. We prescribed pure extract ICKT (TJ-135). ICKT is manufactured by Tsumura Co., Ltd. (Tokyo, Japan) and has been approved as an ethical drug by the Ministry of Health and Welfare of Japan. The daily amount of ICKT is 7.5 g/day in adults. Seven and one-half grams of this product contain 1.5 g of dried extract obtained from mixed raw herbs in the following ratio: 4.0 g of Inchinko (Artemisia Capillaries Spike), 3.0 g of San-shishi (JP Gardenia Fruit), and 1.0 g of Daio (JP Rhubarb Rhizome) [5–8].

Under ether anesthesia, bile duct ligation and SHAM operation were carried out on the rats. After median incision laparotomy, the bile duct was doubly ligated. The SHAM operation involved only an abdominal laparotomy. There were three study groups with eight rats in each. The groups consisted of: (1) SHAM group ($n = 8$), (2) NT-group (no treatment after bile duct ligation) ($n = 8$), and (3) T-group (ICKT treatment group) ($n = 8$). All rats were killed on the 17th postoperative day. Blood was drawn from the inferior vena cava under ether anesthesia, and the livers were removed after ligation of the portal veins, coronary arteries, and inferior vena cava. The livers were fixed in formalin and prepared as specimens, with the exception of about 2.0 g of tissue that was stored frozen at −150° of centigrade in liquid nitrogen immediately after extraction.

The serum AST and ALT levels were measured by a biochemical analysis. Furthermore, the levels of hepatic TGF-beta1 were measured by ELISA method. Immunohistochemical staining of TGF-beta1 in hepatic tissues was performed using mouse anti-human TGF-beta1 monoclonal antibody (Cosmo Bio Co., LTD, Japan) by the ABC method (Vector Laboratories, Burlingame, CA, USA) in order to evaluate the activation of stellate cells. For each specimen, the staining rate was defined as the average TGF-beta1 staining in 5 fields at 400× magnification. The measurements were based on a DI-Ruler (Harada Industry, 1018 Kamimaruko, Ueda-city, Nagano Japan) referring to Kobayashi's method [13].

Real-time PCR (RT-PCR) was performed to evaluate the expression of the tissue inhibitor of metalloproteinase-1 (TIMP-1). The expression level of TIMP-1 was observed to be directly related to the suppression of matrix metalloproteinase [13]. According to Broide, Britton, Lee, and Kobayashi's reports, the expression level of TIMP-1 is endogenous inhibiting factor of MMP group [9–11, 13, 14]. The probes and primers for RT-PCR were obtained from TaqMan™ Gene Expression Assays Realtime TIMP-1 (TIMP-1: Applied Biosystems).

Azan staining and immunohistochemical staining of alfa-smooth muscle actin (alfa-SMA) was performed to evaluate the degree of fibrosis in rats. For each specimen, the staining rate of the positive cells was defined as the average Azan staining in 5 fields at 40× and the average alfa-SMA staining at 100× magnification. The measurements were based on a DI-Ruler.

This animal experimental protocol was approved by the Animal Experiments Committee of Kurume University (No. 2026). The measurements are expressed as the mean ± standard deviation, and comparisons between two groups were performed with the Mann-Whitney U test. p values below 0.05 were considered to be statistically significant.

Results

In the blood biochemical analysis, serum AST was 973.3 ± 212.9 and 579.3 ± 174.3 IU/l in the NT-group and T-group, respectively. The serum ALT was in 279.3 ± 85.2 and 141.2 ± 49.3 IU/l in the NT-group and T-group, respectively. The serum AST and ALT levels in the NT-group were significantly higher than those in the T-group (AST: $p = 0.048$, ALT: $p = 0.046$). Therefore, the administration of ICKT significantly reduced both serum values (Fig. 1).

In TGF-beta1 immunohistochemical staining, the percentages of stained cytoplasm were 22.06 ± 5.4 and

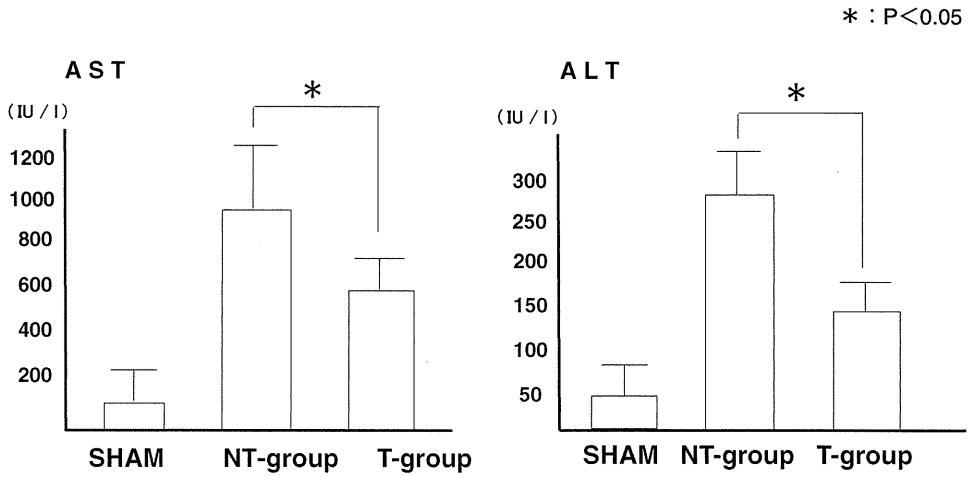

Fig. 1 Serum AST and ALT levels in rats. Serum AST and ALT levels in the NT-group were significantly higher than those in the T-group ($p < 0.05$)

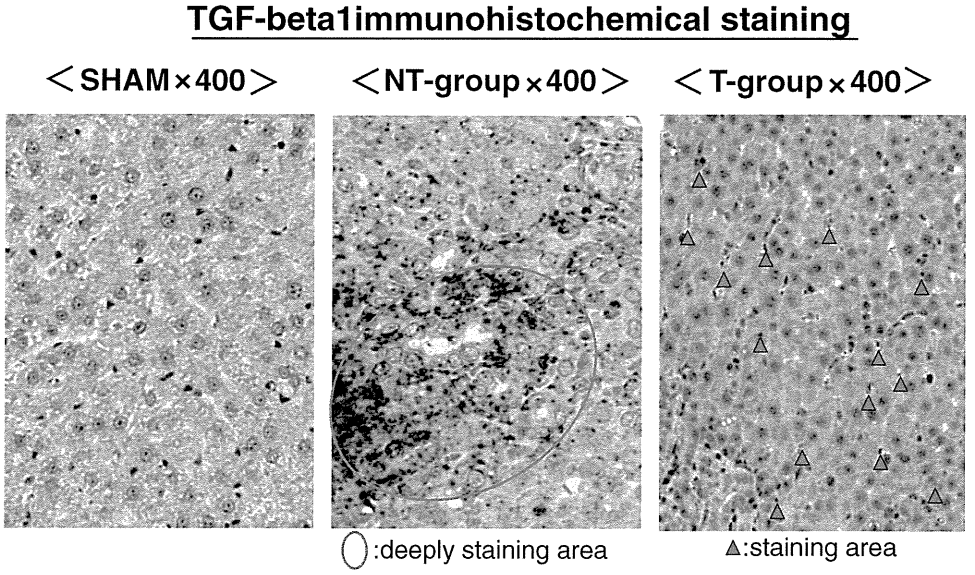

Fig. 2 Immunohistochemical staining of TGF-beta1. The percentages of positive cells were 22.06 ± 5.4 and 0.97 ± 1.45% in the NT-group and T-group, respectively. Staining of TGF-beta1 in the T-group was significantly lower than that in the NT-group ($p < 0.05$)

0.97 ± 1.45% in the NT-group and T-group, respectively ($p = 0.009$, Fig. 2).

Hepatic TGF-beta1 levels were 7.14 ± 1.37 and 2.89 ± 0.79 IU/l in the NT-group and T-group, respectively ($p = 0.008$, Fig. 3).

The relative levels of TIMP-1 m-RNA, indicating the suppression of matrix metalloproteinase, were 76.8 ± 29.5 and 32.7 ± 18.3 times in the NT-group and T-group, respectively, compared to the SHAM group (Fig. 4). Although the relative level of TIMP-1 m-RNA in the T-group was lower than that in the NT-group, there was no significant difference between the two groups.

For alfa-SMA staining, the percentages of positive cells were 47.5 ± 16.4 and 12.4 ± 4.34% in the NT-group and T-group, respectively ($p = 0.009$, Fig. 5). Likewise, Azan staining revealed, fibrotic areas of 33.2 ± 8.5 and 17.3 ± 7.1% in the NT-group and T-group, respectively ($p = 0.0283$). In spite of a high grade of bridging fibrosis in the NT-group, no bridging fibrosis was seen in the T-group (Fig. 6).

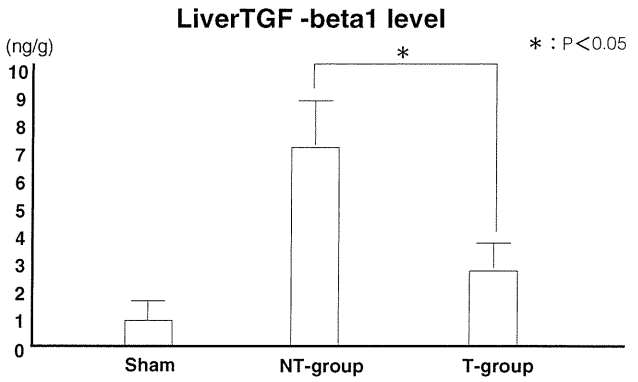

Fig. 3 Hepatic TGF-beta1 levels. The level of hepatic TGF-beta1 in the NT-group was significantly higher than that in the T-group ($p < 0.05$)

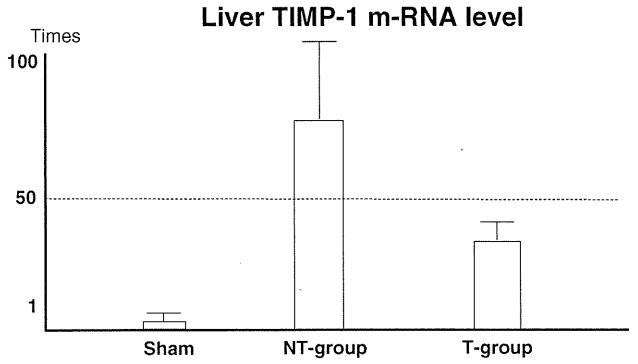

Fig. 4 Hepatic TIMP-1 m-RNA levels. Although the relative quantification of hepatic TMP-1 m-RNA in the T-group was lower than that in the NT-group, there was no significant difference between them

Discussion

Experimental studies have shown that ICKT protects against the hepatic injury induced by various agents in vitro, including alfa-naphtylisothiocyanate, galactosamine, and carbontetrahydrochroride [7]. In addition, recent clinical reports in Japan suggest that ICKT also may be beneficial for the treatment of hepatobiliary diseases such as BA [7, 15]. Several studies have reported ICKT to have an antifibrotic effect, while also improving hepatic injury [6–8, 15, 16]. The models in these reports originate from cholestatic liver disorder, but as a result of injection of carbon tetrachloride (CCl_4), pig-serum, or choline-deficient L-amino acid-deficient diet [6, 8]. We performed bile duct ligation in rats to serve as a model of cholestatic liver disorder, similar to that seen in patients with BA. The aims

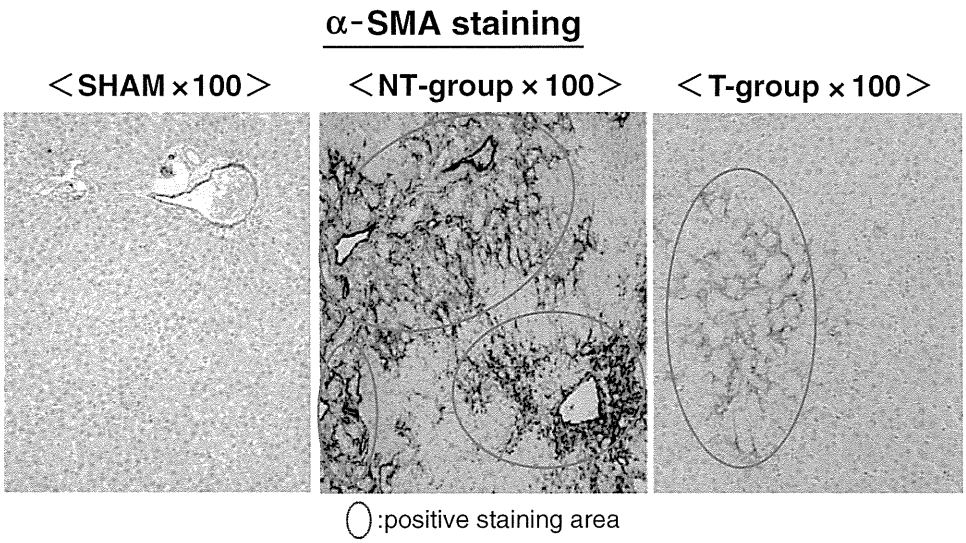

Fig. 5 Immunohistochemical staining of alfa-SMA. The rates of positive cells were 47.5 ± 16.4 and 8.4 ± 4.3% in the NT-group and T-group, respectively. Staining of alfa-SMA in the T-group was significantly lower than that in the NT-group ($p < 0.05$)

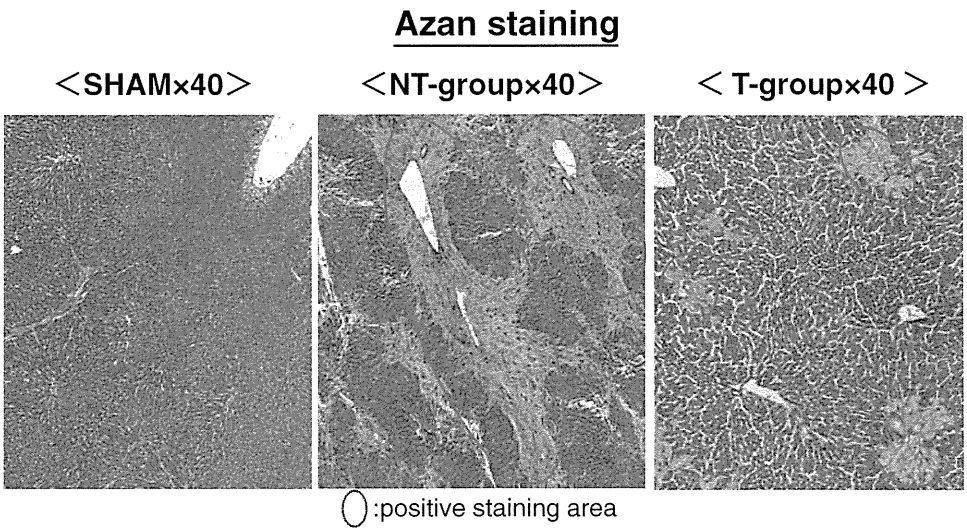

Fig. 6 Azan staining. The percentages of fibrotic areas were 33.2 ± 8.5 and 11.3 ± 7.1% in the NT-group and T-group, respectively. Staining of Azan in the T-group was significantly lower than that in the NT-group ($p < 0.05$). In spite of the high grade of bridging fibrosis in the NT-group, no bridging fibrosis was seen in the T-group

of our study were to confirm both an antifibrotic effect and improvement of hepatic injury by administration of ICKT in cholestatic rats, and to clarify the pharmacodynamic action of ICKT.

By administration of ICKT, we confirmed significant reduction in the serum levels of AST and ALT in cholestatic rats, similar to previous reports [6–8, 15, 16]. The data in these reports confirmed that ICKT also has hepatocyte protective activity in BA patients.

Broide, Britton, and Lee reported that the mechanism of advancing hepatic fibrosis involves activation of stellate cells as a result of continuous inflammation of the liver, which in turn promotes the production of TGF-beta1 and consequently disrupts the balance between production and reduction in the extracellular matrix [9–11]. The pathologic mechanism of the progression from cholestasis to fibrosis might originate from a chemical imbalance in the extracellular matrix caused by the activation of transcription factors and hepatic stellate cells. Continuous inflammation increases the expression of adhesion factors, which results in the accumulation of immune cells in the liver. The subsequent accumulation of hydrophobic bile acid leads to the activation of Kupffer cells [9–11, 14].

Recently, ICKT also has been reported to ameliorate concanavalin A-induced hepatitis by inhibiting the production of inflammatory cytokines [5], through the inhibition of liver cell apoptosis induced by Fas-mediated lethal liver injury [17] and TGF-beta1 [4]. TGF-beta1 is regarded as an undesirable factor in various liver disorders, because this cytokine induces fibrosis in liver tissue and the growth suppression of hepatocytes, which may worsen liver function. Furthermore, the inhibition of TGF-beta1 intervention has been reported to be therapeutic in already-established liver fibrosis, not only by suppressing fibrosis, but also by facilitating hepatocyte regeneration [18]. The reason for the progression of liver fibrosis in many BA patients despite successful surgical treatment remains unclear, but TGF-beta1 has been reported to promote hepatic fibrogenesis via the activation of hepatic stellate cells in BA patients [19].

In our study, there was a significant reduction in hepatic fibrosis in rats given ICKT, as seen both in alfa-SMA staining and Azan staining, compared to the NT-group. To evaluate the hepatic fibrotic mechanism, we investigated the antifibrotic effects by ICKT. In this study, we have shown reduced levels of TGF-beta1 and hepatic TIMP-1 in rats given ICKT.

Yamamoto et al. [4] reported that ICKT reduces the apoptosis of hepatocytes. The significant reductions observed in the serum AST and ALT levels in this study might thus be considered to be hepatocyte protective effects through the prevention of apoptosis by ICKT. However, hepatocytes might instead be protected by the inhibition of TGF-beta1 production due to reduction of hepatic TGF-beta1 levels. ICKT is an aqueous mixture of three herbal extracts: Inchinko (Artemisia Capillaries Spike), San-shishi (JP Gardenia Fruit), Daio (JP Rhubarb Rhizome) in a ratio of 4:3:1 by weight [5–8]. Inchinko and San-shishi are effective for liver disease, and Daio is a laxative and anti-inflammatly agents. Inchinko contains the choleretic agent capillarisin. San-shishi contains genipin, an aglycone converted in the gut from geniposide which has been proven to suppress Fas-induced liver injury in mice [16]. Hepatic fibrosis may have been inhibited due to a reduction of the hepatic TIMP-1 levels, as a marker of the suppression of matrix metalloproteinase, and thus leaded to reduction of TGF-beta1 levels. In this study, we have not yet investigated the transcription factors in the mechanism of hepatic fibrosis. Therefore, further experiments may be necessary to clarify these points.

The excessive production of active-oxygen species might be related to the onset and advancement of hepatic injury, related to continuous intrahepatic inflammation [20]. We have previously reported that postoperative patients with BA were under severe oxidative stress, even with mild liver dysfunction without jaundice [13, 21]. Oxidative stress results in the progression of cholestatic disease, while antioxidant therapy reduces cholestasis [13]. Recently, Nrf2-mediated antioxidant action was reported in cholestatic diseases by administration of ICKT [22]. Therefore, it may be necessary to investigate the effects of ICKT on oxidative stresses from the view point of stress markers in the near future.

In conclusion, the herbal medicine ICKT might protect hepatocytes and reduce fibrosis by suppressing hepatic stellate cell activation and expression level of TIMP-1 in a cholestatic rat model.

References

1. Kiso Y, Ogasawara Y, Hirota K et al (1984) Antihepatotoxic principles of Artemisia capillaris buds. Planta Med 1:81–85234
2. Takeda S, Endo T, Aburada M (1981) Pharmacological studies on iridioid compounds. The choleretic mechanism of iridoid compounds. J Pharmacobiodyn 4:612–623
3. Okuno I, Uchida K, Nakamura M et al (1988) Studies on choleretic constituents in Artemisia capillaris THUMB. Chem Pharmacol Bull 36:769–775
4. Yamamoto M, Ogawa K, Morita M et al (1996) The herbal medicine Inchin-ko-to inhibits liver cell apoptosis inducwd by transforming growth factor beta 1. Hepatology 23:552–559
5. Yamashiki M, Mase A, Arai I et al (2000) Effect of the Japanese herbal medicine Inchinko-to (TJ-135) on concanavalin A-induced hepatitis in mice. Clin Sci 99:421–431
6. Inao M, Mochida S, Matsui A et al (2004) Japanese herbal medicine Inchinko-to as a therapeutic drug for liver fibrosis. J Hepatol 41:584–591

7. Iinuma Y, Kubota M, Yagi M et al (2003) Effects of the herbal medicine Inchinko-to on liver function in postoperative patients with biliary atresia-a pilot study. J Pediatr Surg 38:1607–1611
8. Sakaida I, Tsuchiya M, Kawaguchi K et al (2003) Herbal medicine Inchinko-to (TJ-135) prevents liver fibrosis and enzyme-altered lesions in rat liver cirrhosis induced by a choline-deficient L-amino acid-defined diet. J Hepatol 38:762–769
9. Broide E, Klinowski E, Koukoulis G et al (2000) Superoxide dismutase activity in children with chronic liver diseases. J Hepatol 32:188–192
10. Britton RS, Bacon BR (1994) Role of free radicals in liver diseases and hepatic fibrosis. Hepatogastroenterology 41:343–348
11. Lee KS, Buck M, Houglum K et al (1995) Activation of hepatic stellate cells by TGF alpha and collagen type I is mediated by oxidative stress through c-myb expression. J Clin Invest 96: 2461–2468
12. Imanishi T, Maeda N, Otogawa K et al (2004) Herb medicine Inchin-ko-to (TJ-135) regulates PDGF-BB-dependent signaling pathways of hepatic stellate cells in primary culture and attenuates development of liver fibrosis induced by thioacetamide administration in rats. J Hepatol 41:242–250
13. Kobayashi H, Tanaka Y, Asagiri K et al (2010) The antioxidant effect of green tea catechin ameliorates experimental liver injury. Phytomedicine 17:197–202
14. Wells RG (2000) Fibrosis.V. TGF-beta signaling pathways. Am J Physiol Gastrointest Liver Physiol 279:845–850
15. Kobayashi H, Horikoshi K, Yamataka A et al (2001) Beneficial effect of a traditional herbal medicine (inchin-ko-to) in postoperative biliary atresia patients. Pediatr Surg Int 17:386–389
16. Tamura T, Kobayashi H, Yamataka A et al (2007) Inchin-ko-to prevents medium-term liver fibrosis in postoperative biliary atresia patients. Pediatr Surg Int 23:343–347
17. Yamamoto M, Miura N, Ohtake N et al (2000) Genipin, a metabolic derived from the herbal medicine Inchin-ko-toand suppression of Fas-induced lethal liver apoptosis in mice. Gastroenterology 118:380–389
18. Nakamura T, Sakata R, Ueno T et al (2000) Inhibition of transforming growth factor beta prevents progression of liver fibrosis and enhances hepatocyte regeneration in dimethlnitrosoamine-treated rats. Hepatology 32:247–255
19. Ramm GA, Nair VG, Bridle KR et al (1998) Contribution of hepatic parenchymal and non parenchymal cells to hepatic fibrosis in biliary atresia. Am J Pathol 153:527–535
20. Baskol G, Baskol M, Kocer D (2007) Oxidative stress and antioxidant defenses in serum of patients with non-alcoholic steatohepatitis. Clin Biochem 40:776–780
21. Asakawa T, Tanaka Y, Asagiri K et al (2009) Oxidative stress profile in the post-operative patients with biliary atresia. Pediatr Surg Int 25:93–97
22. Okada K, Shoda J, Kano M et al (2007) Inchinkoto, a herbal medicine, and its ingredients dually exert Mrp2/MRP2-mediated choleresis and Nrf2-mediated antioxidative action in rat livers. Am J Physiol Gastrointest Liver Physiol 292:1450–1463

INTERNAL MEDICINE

□ CASE REPORT □

Focal Nodular Hyperplasia-Like Nodule with Reduced Expression of Organic Anion Transporter 1B3 in Alcoholic Liver Cirrhosis

Nobuko Doi[1], Yasuyuki Tomiyama[1], Tomoya Kawase [1], Sohji Nishina[1], Naoko Yoshioka[1], Yuichi Hara[1], Koji Yoshida[1], Keiko Korenaga[1], Masaaki Korenaga[1], Takuya Moriya[2], Atsushi Urakami[3], Osamu Nakashima[4], Masamichi Kojiro[4] and Keisuke Hino[1]

Abstract

We report a patient with alcoholic liver cirrhosis who had a 15 mm focal nodular hyperplasia (FNH)-like nodule in the liver. This FNH-like nodule was diagnosed as hepatocellular carcinoma (HCC) mainly based on hypervascularity during the hepatic arterial phase, washout pattern during the equilibrium phase and low signal intensity during the hepatobiliary phase in gadolinium-ethoxybenzyl-diethylenetriamine pentaacetic acid (Gd-EOB-DTPA)-enhanced MRI; it was surgically resected. Its histology exhibited hepatocyte hyperplasia, fibrous septa containing unpaired small arteries accompanied by reactive bile ductules, remarkable iron deposits and sinusoidal capillarization, and was compatible with the diagnosis of an FNH-like nodule. When we analyzed the images of the present nodule retrospectively, low signal intensity on in-phase and isosignal intensity on opposed-phase T1-weighted MRI may have reflected iron deposits in the FNH-like nodule. In addition, a low signal intensity on T2-weighted MRI and no detection in diffusion-weighted MRI may help in distinguishing FNH-like nodules from HCC, since these image findings are inconsistent with typical HCC. Immunohistochemical analysis revealed a markedly reduced expression of organic anion transporter (OATP) 1B3 in this nodule, which implied decreased Gd-EOB-DTPA uptake by hepatocytes and accounted for the low signal intensity during the hepatobiliary phase on Gd-EOB-DTPA-enhanced MRI. To the best of our knowledge this is the first report in which an FNH-like nodule was assessed for OATP1B3 expression.

Key words: alcoholic liver cirrhosis, FNH-like nodule, hepatocellular carcinoma, organic anion transporter, Gd-EOB-DTPA-enhanced MRI

(Intern Med 50: 1193-1199, 2011)
(DOI: 10.2169/internalmedicine.50.4637)

Introduction

Due to improvements in imaging techniques and pathological evaluation, a new type of small focal lesion occurring in the cirrhotic liver has been described (1-3). Focal nodular hyperplasia (FNH)-like nodules (FNH-like nodules) are focal lesions occurring in liver cirrhosis and are morphologically very similar to classical FNH in the otherwise normal liver. In general, FNH-like nodules are assumed not to have an increased risk of malignant transformation (1-3), but this issue remains elusive (4). FNH-like nodules are occasionally misdiagnosed on imaging as hepatocellular carcinoma (HCC) due to hypervascularity during the arterial phase of magnetic resonance imaging (MRI)/computed tomography (CT).

On the other hand, gadolinium-ethoxybenzyl-diethylenetriamine pentaacetic acid (Gd-EOB-DTPA)-

[1]Departments of Hepatology and Pancreatology, Kawasaki Medical University, Japan, [2]Department of Pathology, Kawasaki Medical University, Japan, [3]Department of Digestive Surgery, Kawasaki Medical University, Japan and [4]Department of Pathology, Kurume University School of Medicine, Japan
Received for publication October 5, 2010; Accepted for publication December 17, 2010
Correspondence to Dr. Keisuke Hino, khino@med.kawasaki-m.ac.jp

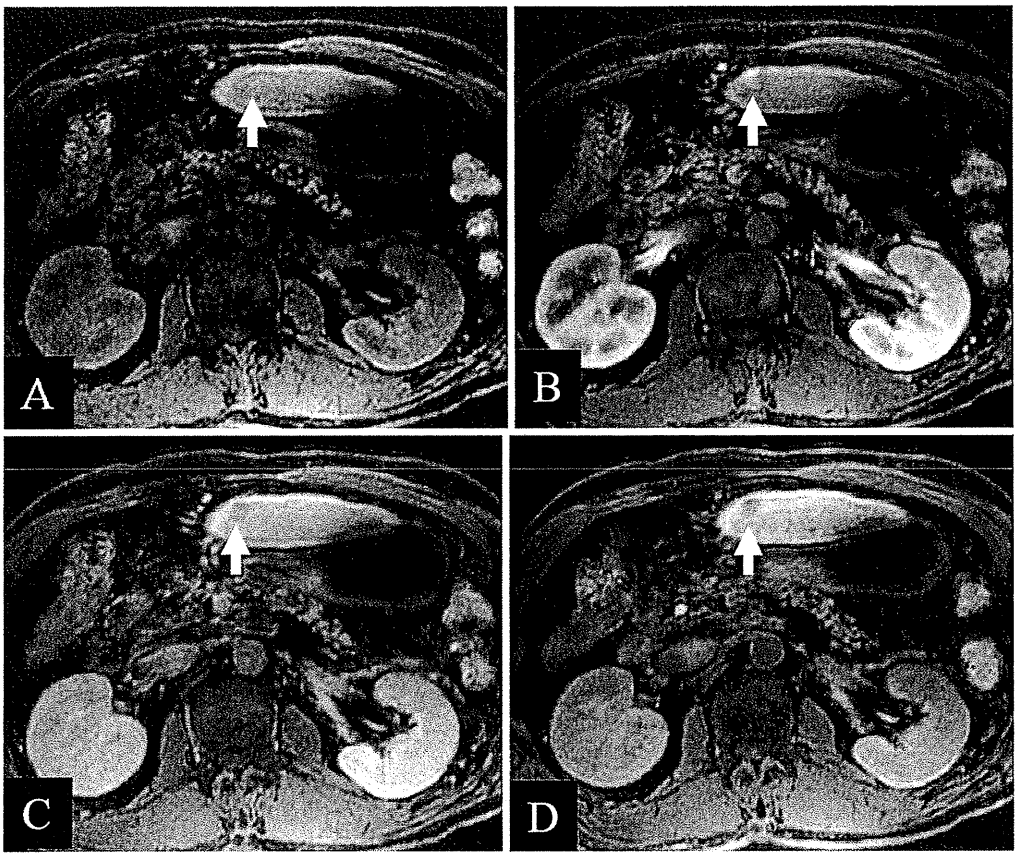

Figure 1. Images of the FNH-like nodule in segment 3 in Gd-EOB-DTPA-enhanced MRI. Arrows indicate a 9mm FNH-like nodule. (A) Low signal intensity before contrast injection, (B) High signal intensity during the hepatic arterial phase, (C) Washout pattern during the equilibrium phase, (D) Low signal intensity during the hepatobiliary phase.

enhanced MRI has enabled us to detect focal liver lesions because of its hepatocyte-specific properties (5-7), and it might be the most useful imaging modality for the diagnosis of HCC at present (8, 9). However, the image findings of FNH-like nodules in Gd-EOB-DTPA-enhanced MRI are not well known, and it remains unclear if FNH-like nodules can be distinguished from HCC in Gd-EOB-DTPA-enhanced MRI. Here, we report a histologically proven FNH-like nodule in a patient with alcoholic liver cirrhosis, and discuss the diagnostic potential of Gd-EOB-DTPA-enhanced MRI for FNH-like nodules.

Case Report

A 68-year-old Japanese man with a history of alcoholic liver cirrhosis for approximately 10 years was found to have a 9 mm hypervascular nodule in the liver through contrast-enhanced CT and admitted to Kawasaki Medical University Hospital in June 2008 for further examination of the hepatic nodule.

His alcoholic consumption over the previous 40 years was 100 g or more per day. A physical examination on admission showed no remarkable abnormalities except for moderate splenomegaly. Laboratory data on admission disclosed the following abnormal values: platelet count $9.4\times10^4/\mu L$ (normal range 15-35), aspartate aminotransferase 58 IU/L (10-35), γ-glutamyl transpeptidase 346 IU/L (5-60) and indocyanine green retention rate at 15 minutes 16.4% (<10). The levels of hepatic tumor markers were as follows: α-fetoprotein 9.0 ng/mL (<10) and des-γ-carboxy prothrombin 25 mAU/mL (<40). The serum was negative for anti-hepatitis C virus antibody and hepatitis B surface (HBs) antigen but positive for anti-HBs and anti-hepatitis B core antibodies.

Neither B-mode sonographic scans nor Sonazoid contrast-enhanced ultrasonography detected the hepatic nodule. Arteriography did not disclose any hypervascular mass lesion. Contrast-enhanced CT revealed a nodule of 9 mm in the liver segment 3 as hypervascularity during the hepatic arterial phase. Gd-EOB-DTPA-enhanced MRI disclosed that this nodule had a low signal intensity before contrast injection (Fig. 1A), hypervascularity during the hepatic arterial phase (Fig. 1B), a washout pattern during the equilibrium phase (Fig. 1C), and a low signal intensity during the hepatobiliary phase (Fig. 1D). Diffusion-weighted MRI did not reveal this nodule (Fig. 2A). In- and opposed-phase T1-weighted MRI, and T2-weighted MRI disclosed this nodule as low signal intensity (Fig. 2B), isosignal intensity (Fig. 2C) and slightly

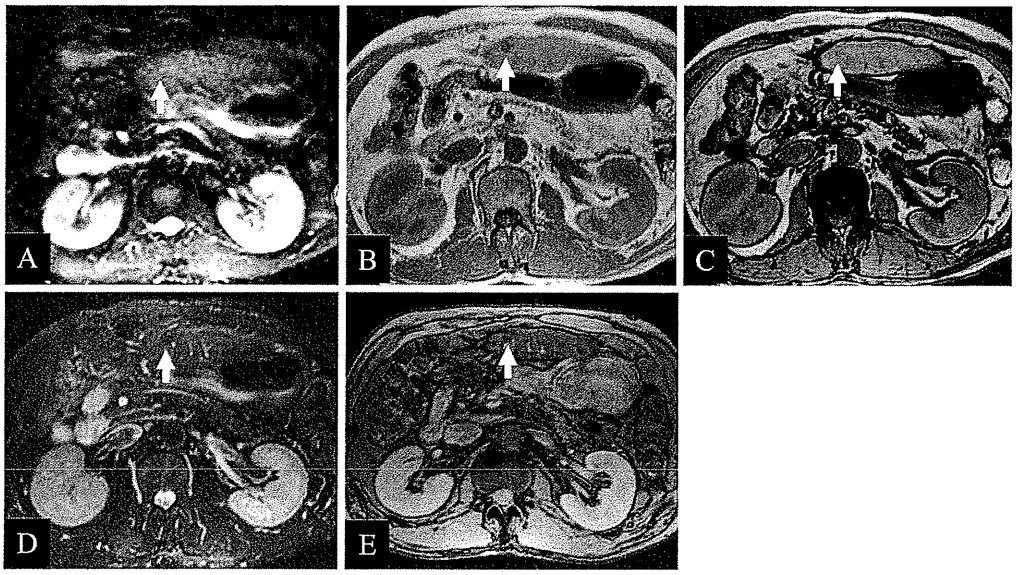

Figure 2. Images of the FNH-like nodule in segment 3 in Gd-EOB-DTPA-enhanced MRI. Arrows indicate the 9mm FNH-like nodule. (A) No detection of nodule in diffusion-weighted MRI, (B) Low signal intensity on in-phase T1-weighted MRI, (C) Isosignal intensity on opposed-phase T1-weighted MRI, (D) Slightly low signal intensity in T2-weighted MRI, (E) Slightly low signal intensity in SPIO-enhanced MRI.

low signal intensity (Fig. 2D), respectively. Although this nodule was detected as slightly low signal intensity (Fig. 2E) in superparamagnetic iron oxide (SPIO)-enhanced MRI, it was uncertain if Kupffer cells took up SPIO because of the slightly low signal intensity on T2-weighted MRI before SPIO injection.

The imaging findings mentioned above were suggestive of HCC, even though several findings, such as low signal intensity on in-phase and isosignal intensity on opposed-phase T1-weighted MRI, low signal intensity in T2-weighted MRI and no detection in diffusion-weighted MRI, were not consistent with typical HCC. We could not histologically assess this hepatic nodule by liver biopsy because of its undetectability by ultrasonography, and we could not ignore the possibility of HCC as the diagnosis of this nodule. Therefore, this nodule was surgically resected after obtaining informed consent from the patient. The nodule of interest was not encapsulated and its margin was difficult to distinguish from the surrounding cirrhotic tissue (Fig. 3A and 3B). Intranodular fibrous septa were present but central fibrous scarring and portal tracts were absent (Fig. 3C). The fibrous septa contained unpaired small arteries accompanied by reactive bile ductules radiating into the parenchyma (Fig. 3D). This nodule showed varying degrees of increased cellularity (Fig. 4A) and marked iron deposits in the hepatocyte and/or Kupffer cells (Fig. 4B) compared to the surrounding cirrhotic tissue. Immunohistochemical analysis using an anti-CD34 antibody (anti-CD34) revealed marked sinusoidal capillarization (Fig. 4C). Thus, the histological diagnosis of this nodule was an FNH-like nodule. Finally, we immunohistochemically assessed the expression of organic anion transporter (OATP) 1B3 in hepatocytes, using an anti-OATP1B3 antibody (anti-OATP1B3) to examine why this nodule exhibited low signal intensity during the hepatobiliary phase of Gd-EOB-DTPA-enhanced MRI. Immunohistochemically, OATP1B3 was diffusely and strongly positive for the cell membrane of the hepatocytes in the surrounding cirrhotic tissue, but was nearly absent in the FNH-like nodule (Fig. 5A-C). Thus far neither recurrence of the FNH-like nodule nor the development of HCC has been found in this patient who has stopped drinking alcohol since he was admitted to our hospital.

Discussion

FNH-like nodules occurring in cirrhotic livers are reported to have the pathological features such as encapsulation, hepatocyte hyperplasia, fibrous septa containing unpaired small arteries accompanied by reactive bile ductules, iron deposits and/or sinusoidal capillarization (1, 2). It has been suggested that the artery-dominant condition derived from disturbed portal circulation in the cirrhotic liver (10) or the congenital vascular anomaly (11, 12) causes localized hyperplastic changes of the hepatocytes, and generates nodular lesions such as FNH. The increased unpaired arteries, diffuse capillarization, and iron deposits in the nodule would be attributable to a similar mechanism in nodular formation. The FNH-like nodule in this study had these pathological features except for encapsulation. One possible explanation for the lack of encapsulation is that hepatocytic hyperplasia had not expanded sufficiently to be encapsulated because it was the early stage in the development of the hyperplastic nod-

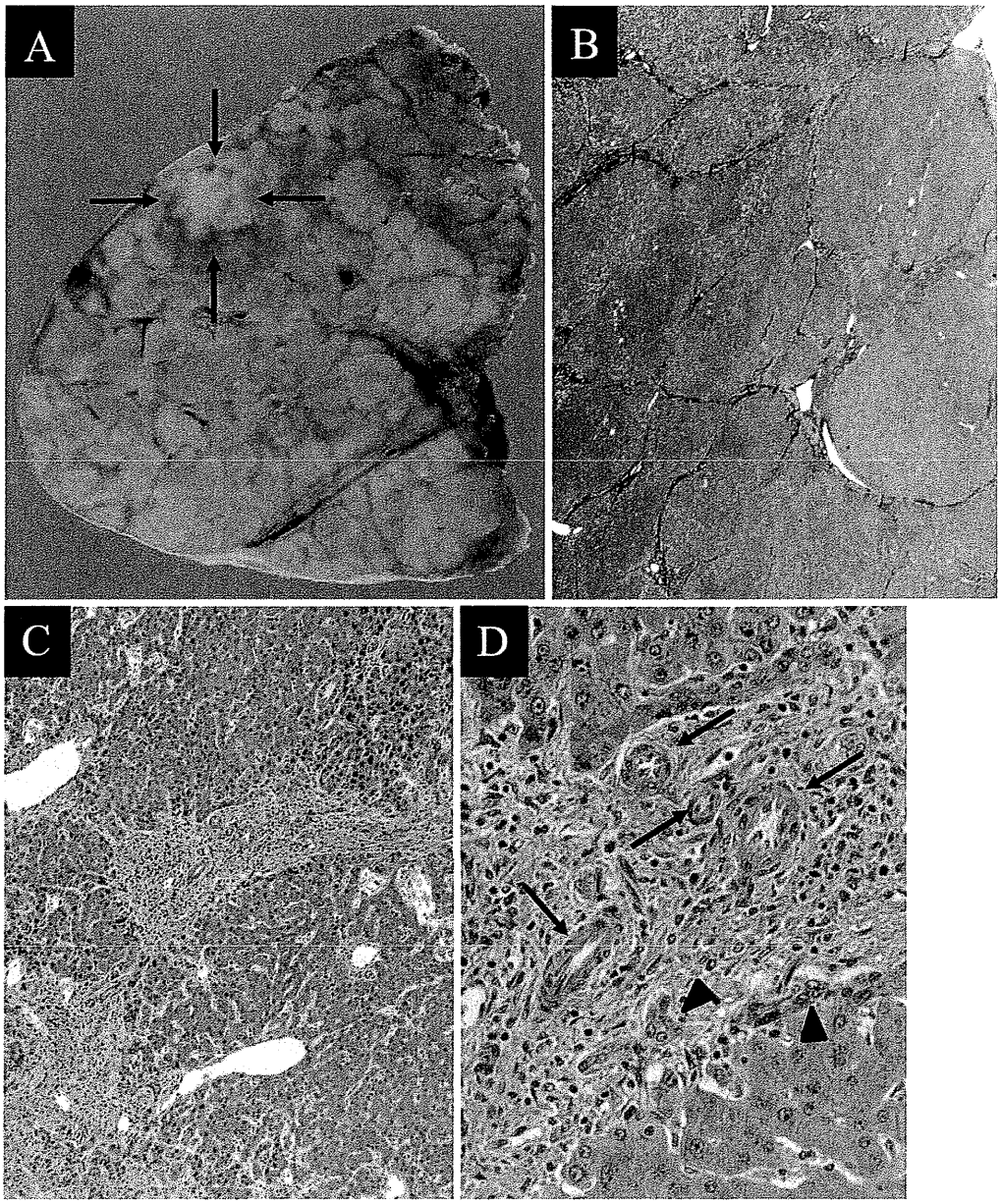

Figure 3. Surgically resected specimen and histology of the FNH-like nodule. (A) Arrows indicate the FNH-like nodule (15mm). The nodule is not encapsulated and its margin is difficult to distinguish from the surrounding tissue. (B) The surrounding tissue shows liver cirrhosis (Masson trichrome ×40). (C) Fibrovascular septa with mild lymphocyte infiltrate within the FNH-like nodule (Hematoxylin and Eosin staining ×100), (D) Unpaired small arteries (arrows) and reactive bile ductules radiating into the parenchyma (arrowheads) within a fibrovascular septum in the FNH-like nodule (Hematoxylin and Eosin staining ×400).

ule. In this respect the state of the present FNH-like nodule may suggest its early stage. The present case clearly indicated the existence of an FNH-like nodule with reduced OATP1B3 expression. Hepatocytic disorder derived from disturbed portal circulation in cirrhotic liver may have suppressed the expression of OATP1B3. We cannot necessarily exclude a possibility of malignant potential of this nodule in terms of nearly absent expression of OATP1B3. Otherwise, unknown mechanisms may have been related to the reduced expression of OATP1B3.

FNH-like nodules also are clinically important lesions in terms of difficulty in distinguishing them from well-differentiated HCC in image diagnosis. There were at least two reasons why we had diagnosed this patient as having probable HCC in imaging. First, the present FNH-like nodule exhibited hypervascularity during the hepatic arterial phase and a washout pattern during the equilibrium phase in contrast-enhanced MRI. Second, the Gd-EOB-DTPA-enhanced MRI revealed this nodule to have low signal intensity during the hepatobiliary phase, which implied re-

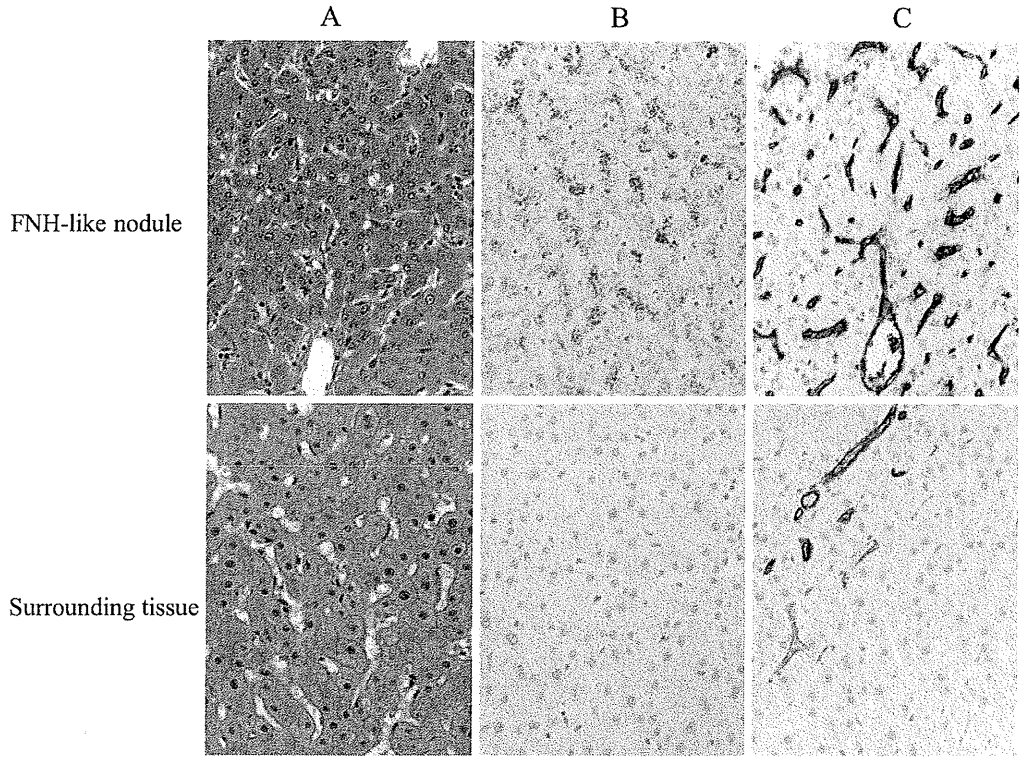

Figure 4. Cell density, iron deposits and sinusoidal capillarization in the FNH-like nodule and the surrounding tissue. The FNH-like nodule shows increased cell density (A, Hematoxylin and Eosin staining ×400), remarkable iron deposits in the hepatocyte and/or Kupffer cells (B, Berlin blue ×400) and marked sinusoidal capillarization (C, immunohistochemical staining using anti-CD34 ×400), compared to the surrounding tissue.

duced uptake of Gd-EOB-DTPA by hepatocytes. Reduced Gd-EOB-DTPA uptake by hepatocytes was reported to suggest an early event of hepatocarcinogenesis in a recent study (13). In contrast, FNH is demonstrated to be enhanced during the hepatobiliary phase of Gd-EOB-DTPA-enhanced MRI (5, 14). With respect to this point, it should be noted that the present FNH-like nodule may have had an exceptionally low signal intensity during the hepatobiliary phase. The present results were consistent with the recent report that uptake of Gd-EOB-DTPA is determined by OATP1B3 expression rather than by tumor differentiation or bile production in HCC (15), and suggested the difficulty in discriminating between FNH-like nodules and HCC by assessing the Gd-EOB-DTPA uptake by hepatocytes.

Which MRI imaging findings were useful for distinguishing between FNH-like nodules and HCC in this patient? When we analyzed the images of this nodule retrospectively, there seemed to be three important findings for diagnosis. First, the low signal intensity on in-phase and isosignal intensity on opposed-phase T1-weighted MRI may have reflected iron deposits in the FNH-like nodule, since similar phase-shift imaging has been reported to reflect hemosiderin deposits in regenerative nodules in liver cirrhosis (16). In contrast, the isointensity to slightly high intensity on in-phase and the low signal intensity on opposed-phase T1-weighted MRI are known to reflect hepatocellular nodules with fatty degeneration (8). Thus, the combined findings from the in-phase and opposed-phase may facilitate discrimination between FNH-like nodules and well-differentiated HCC, since the former frequently have iron deposits and the latter has fatty degeneration. Second, FNH-like nodules and HCC have been shown to be likely to exhibit iso- to low signal intensity and high signal intensity in T2-weighted MRI, respectively (17), which was consistent with the low signal intensity in the present nodule. Third, the lack of detection in diffusion-weighted MRI may help in distinguishing FNH-like nodules from HCC, since diffusion-weighted MRI imaging has been reported to be useful in differentiating benign hepatocellular nodules including FNH from HCC (18). However, it still may be difficult to distinguish such small FNH-like nodules showing low signal intensity during the hepatobiliary phase in Gd-EOB-DTPA-enhanced MRI from HCC in clinical practice.

In addition, it remains controversial whether FNH-like nodules can be distinguished from HCC based on the presence of Kupffer cells in the nodules. A defect in the Kupffer phase on contrast-enhanced ultrasonography, which implies the absence of Kupffer cells, has been reported in the FNH-like nodule in alcoholic liver cirrhosis (19), whereas the presence of Kupffer cells on SPIO-enhanced MRI has also been shown in FNH-like nodules in alcoholic liver cirrhosis (17). The present FNH-like nodule may have contained

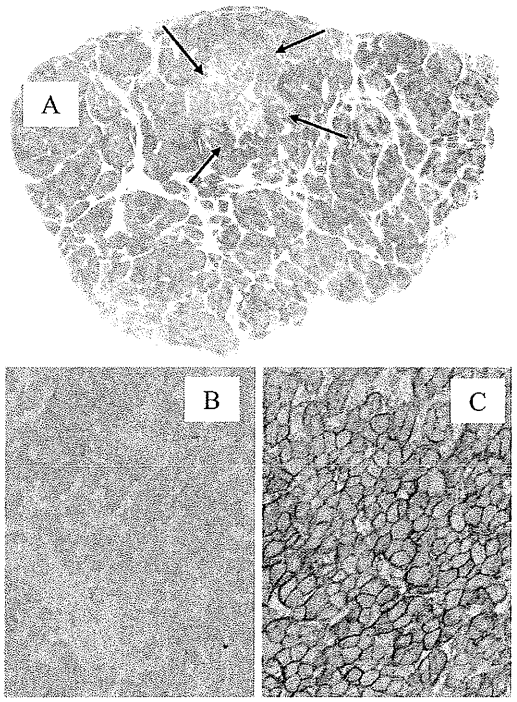

Figure 5. Expression of OATP1B3 in surgically resected specimen. Arrows indicate the FNH-like nodule (A). The expression of OATP1B3 is nearly absent in the nodule (B, ×400), but is diffusely found in the surrounding tissue (C, ×400). OATP1B3 was immunohistochemically detected using anti-OATP1B3.

Kupffer cells, since Sonazoid contrast-enhanced ultrasonography did not detect this nodule. However, we could not precisely assess the uptake of SPIO by Kupffer cells because of the slightly low signal intensity on T2-weighted MRI before SPIO injection. Thus, the present case suggests the importance of pathological diagnosis for hepatic small nodular lesions as well as the difficulty in image diagnosis for such lesions. We also propose that observational follow-up is also an important modality to be chosen when nodules are less than 1.5 cm in diameter, since small nodular lesions associated with chronic liver diseases smaller than 1.5 cm have been reported to have less potential to be early HCC (20).

In conclusion, we found an FNH-like nodule with reduced expression of OATP1B3 in a patient with alcoholic liver cirrhosis, and retrospectively analyzed imaging findings useful for distinguishing FNH-like nodules from HCC.

The authors state that they have no Conflict of Interest (COI).

Acknowledgement

This study was supported by a grant from the Ministry of Education, Culture, Sports, Science and Technology (No. 20590782), and in part by a Research on Hepatitis, Health and Labor Sciences Research Grants from the Ministry of Health, Labor and Welfare, Japan.

References

1. Quaglia A, Tibballs J, Grasso A, et al. Focal nodular hyperplasia-like areas in cirrhosis. Histopathology **42**: 14-21, 2003.
2. Nakashima O, Kurogi M, Yamaguchi R, et al. Unique hypervascular nodules in alcoholic liver cirrhosis: identical to focal nodular hyperplasia-like nodules? J Hepatol **41**: 992-998, 2004.
3. Libbrecht L, Cassiman D, Verslype C, et al. Clinicopathological features of focal nodular hyperplasia-like nodules in 130 cirrhotic explant livers. Am J Gastroenterol **101**: 2341-2346, 2006.
4. Ishak KG, Goodman ZD, Stocker JT. Tumor of the liver and intrahepatic bile ducts. In: Atlas of Tumor Pathology, 3rd ser. Craig JR, Peters RL, Edmondson HA, Eds. Armed Forces Institute of Pathology, Washington DC, 2001: 38.
5. Huppertz A, Haraida S, Kraus A, et al. Enhancement of focal liver lesions at gadoxetic acid-enhanced MR imaging: correlation with histopathologic findings and spiral CT--initial observations. Radiology **234**: 468-478, 2005.
6. Saito K, Kotake F, Ito N, et al. Gd-EOB-DTPA enhanced MRI for hepatocellular carcinoma: quantitative evaluation of tumor enhancement in hepatobiliary phase. Magn Reson Med Sci **4**: 1-9, 2005.
7. Kim SH, Kim SH, Lee J, et al. Gadoxetic acid-enhanced MRI versus triple-phase MDCT for the preoperative detection of hepatocellular carcinoma. AJR Am J Roentgenol **192**: 1675-1681, 2009.
8. Ichikawa T. MRI in the evaluation of hepatocellular nodules: role of pulse sequences and contrast agents. Intervirology **47**: 252-270, 2004.
9. Kanematsu M, Kondo H, Goshima S, Tsuge Y, Watanabe H. Magnetic resonance imaging of hepatocellular carcinoma. Oncology **75** (Suppl 1): 65-71, 2008.
10. Wanless IR, Mawdsley C, Adams R. On the pathogenesis of focal nodular hyperplasia of the liver. Hepatology **5**: 1194-1200, 1985.
11. Kondo F. Benign nodular hepatocellular lesions caused by abnormal hepatic circulation: etiological analysis and introduction of a new concept. J Gastroenterol Hepatol **16**: 1319-1328, 2001.
12. Kondo F. Focal nodular hyperplasia-like lesions in heavy drinkers. Intern Med **48**: 1117-1123, 2009.
13. Kogita S, Imai Y, Okada M, et al. Gd-EOB-DTPA-enhanced magnetic resonance images of hepatocellular carcinoma: correlation with histological grading and portal blood flow. Eur Radiol **20**: 2405-2413, 2010.
14. Zech CJ, Grazioli L, Breuer J, Reiser MF, Schoenberg SO. Diagnostic performance and description of morphological features of focal nodular hyperplasia in Gd-EOB-DTPA-enhanced liver magnetic resonance imaging: results of a multicenter trial. Invest Radiol **43**: 504-511, 2008.
15. Narita M, Hatano E, Arizono S, et al. Expression of OATP1B3 determines uptake of Gd-EOB-DTPA in hepatocellular carcinoma. J Gastroenterol **44**: 793-798, 2009.
16. Ohtomo K, Itai Y, Ohtomo Y, Shiga J, Lio M. Regenerating nodules of liver cirrhosis: MR imaging with pathologic correlation. AJR Am J Roentgenol **154**: 505-507, 1990.
17. Kobayashi S, Matsui O, Kamura T, et al. Imaging of benign hypervascular hepatocellular nodules in alcoholic liver cirrhosis: differentiation from hypervascular hepatocellular carcinoma. J Comput Assist Tomogr **31**: 557-563, 2007.
18. Taouli B, Vilgrain V, Dumont E, Daire JL, Fan B, Menu Y. Evaluation of liver diffusion isotropy and characterization of focal hepatic lesions with two single-shot echo-planar MR imaging sequences: prospective study in 66 patients. Radiology **226**: 71-78, 2003.
19. Kim SR, Imoto S, Ikawa H, et al. Focal nodular hyperplasia-like lesion with venous washout in alcoholic liver cirrhosis. Intern Med **47**: 1899-1903, 2008.
20. Sakamoto M, Hirohashi S, Shimosato Y. Early stages of multistep

hepatocarcinogenesis: adenomatous hyperplasia and early hepatocellular carcinoma. Hum Pathol **22**: 172-178, 1991.